Publ. Astron. Soc. Japan **42**, 1–17 (1990)

CO Line Observations of the Bar and Nucleus of the Barred Spiral Galaxy M83*

Toshihiro HANDA† and Naomasa NAKAI[1]

Nobeyama Radio Observatory,
Minamimaki-mura, Minamisaku-gun, Nagano 384-13[2]

Yoshiaki SOFUE

Institute of Astronomy, Faculty of Science, The University of Tokyo,
Mitaka, Tokyo 181

Masahiko HAYASHI

Department of Astronomy, Faculty of Science, The University of Tokyo,
Bunkyo-ku, Tokyo 113

and

Mitsuaki FUJIMOTO

Department of Physics, Faculty of Science, Nagoya University,
Chikusa-ku, Nagoya 464-01

(Received 1988 August 17; accepted 1989 August 30)

Abstract

CO ($J = 1 - 0$) line observations of the bar and nucleus of the intermediate barred spiral galaxy M83 were made with the 45-m telescope of the Nobeyama Radio Observatory with a 16″-beam. The observed area was 210″ × 60″(3.8 kpc × 1.1 kpc), which covered the optical bar. A ridge of CO emission is found on the leading edge of the bar and is traced by straight dust lanes. In the mapped field, about 40 % of the CO line flux is concentrated within a radius of 0.4 kpc around the center of the galaxy. The velocity field suggests a noncircular motion of the gas, which

[1]*This work was carried out under the common-use observation program at the Nobeyama Radio Observatory (NRO). NRO is a branch of the National Astronomical Observatory, an inter-university research institute operated by the Ministry of Education, Science, and Culture.

[2]†Present address: Institute of Astronomy, Faculty of Science, The University of Tokyo, Mitaka, Tokyo 181.

is consistent with the prediction by the theoretical models for barred spiral galaxies. The CO line profiles suggest that the rotation curve rises steeply in the nucleus and that the velocity dispersion is 50–100 km s^{-1} around the nucleus.

Key words: Barred spiral galaxies; Molecular gas; Noncircular motion; Star formation.

1. Introduction

The distribution and kinematics of interstellar gas in a galactic disk with a barred potential have been theoretically studied by several investigators (Sørensen et al. 1976; Huntley et al. 1978; Roberts et al. 1979; Prendergast 1983, and the references therein). Numerical simulations and analytic solutions predict that the bar potential forms a shock wave of gas on the leading edge of the bar. At the shock front, the interstellar gas is compressed and loses kinetic energy, resulting in an inflow toward the nucleus. The star forming activity in the nucleus of barred spiral galaxies is thought to be triggered by such a gas inflow (e.g., Sørensen et al. 1976). In order to confirm the scenario, investigations of the distribution and kinematics of molecular clouds, which are tightly correlated to star-formation, in bared spiral galaxies are needed. However, few molecular line observations of a bar have yet been made.

M83 (=NGC 5236) is one of the nearest galaxies with a pronounced bar structure. Its distance has been estimated to be 3.7 Mpc (de Vaucouleurs 1979). The morphological type of M83 is an intermediate barred spiral, SAB(s)c I-II, and the inclination is 24° (face-on = 0°) (de Vaucouleurs et al. 1983). Parameters of M83 are summarized in table 1.

Evidence for active star formation in the central region of M83 has been given by extensive observations at various frequencies. The nucleus shows complex structure at optical wavelengths and has been called "amorphous" (Sérsic and Pastoriza 1965; Pastoriza 1975). The size in blue light is about 20″–30″ in diameter. The emission at 10 μm was detected from an extended region of about 12″ diameter (Rieke 1976). Strong ultraviolet (UV) radiation was detected at the nucleus and at some luminous

Table 1. The galaxy parameters.

Parameter		Value
Center position[a]	R.A. (1950.0)	$13^h34^m11^s.55$
	Decl. (1950.0)	−29°36′42″.2
Systemic Velocity (V_{LSR})[b]		510 km s^{-1}
Morphological type[c]		SAB(s)c I-II
Distance[d]		3.7 Mpc
Inclination[e]		24° (face-on = 0°)
Position Angle[e]		45°
Beam size on galaxy(16″)		290 pc

[a] Rumstay and Kaufman 1983.
[b] This paper.
[c] de Vaucouleurs et al. 1976 (RC2).
[d] de Vaucouleurs 1979.
[e] Comte 1981.

spots on the spiral arms. The UV radiation from the nucleus extends to about 5″–10″ (Bohlin et al. 1983). On the contrary, little UV emission was detected from the bar. Radio continuum radiation and Hα emission show extended structures around the nucleus as well as an elongated ridge along the dust lanes [radio continuum: Ondrechen (1985), Hα: Talbot et al. (1979)]. These results suggest vigorous star-forming activity within the nuclear region, but not so strong along the bar.

CO ($J = 1 - 0$) observations of M83 have previously been made by Rickard et al. (1977) and Combes et al. (1978) using the 11-m telescope at the National Radio Astronomy Observatory (NRAO) with a 64″-beam. They found strong CO emission concentrated in the nuclear region. Using the 14-m telescope at the Five College Radio Astronomy Observatory Lord et al. (1987) observed the galaxy with a 45″-beam. They found a "molecular bar" along the major axis of the optical bar of the galaxy. However, their angular resolutions were insufficient to resolve the spatial distribution and the kinematics of the CO gas in the bar (the bar size is about $2' \times 0.'5$). In order to investigate the behavior of the molecular gas under the existence of a bar potential, we conducted high-resolution ^{12}CO($J = 1 - 0$) line observations.

2. Observations

The observations were made during April and May 1985, and January, March, and April 1986 using the 45-m telescope at the Nobeyama Radio Observatory (NRO). The observed line was the ^{12}CO($J = 1 - 0$) molecular line at 115.27 GHz. A cooled Schottky-barrier diode mixer receiver was attached to a 2048-channel acousto-optical spectrometer. The half-power beam width (HPBW) was 16″, corresponding to 290 pc at the distance of 3.7 Mpc. The instantaneous frequency coverage of the spectrometer was 250 MHz, corresponding to 650 km s^{-1} at 115 GHz. The velocity resolution was 0.64 km s^{-1} on the spectrometer. In order to improve the signal-to-noise ratio, we averaged every 32-channels of the original spectra, yielding a resultant velocity resolution of about 10 km s^{-1}. The observations were made at 20°–25° elevation. The system noise temperature corrected for the atmospheric attenuation was about 1500 K in 1985 and 1200 K in 1986 at 20° elevation. The rms noise temperature was typically 0.03 K to 0.07 K for the 10-km s^{-1} velocity resolution. The aperture efficiency ($\eta_{\rm a}$) and the main beam efficiency ($\eta_{\rm mb}$) were 0.25 and 0.3 in 1985, respectively, and 0.26 and 0.45 in 1986, respectively. The improvement of the beam efficiency was due to an improvement in the subreflector during the summer of 1985.

In order to reduce the overhead time for observations we used common off-source position data for every three on-source position data. The center position of the map was taken at $\alpha = 13^{\rm h}34^{\rm m}11^{\rm s}.55$, $\delta = -29°36'42''.2$ (epoch 1950.0), which is the central position of M83 defined by optical observations (Rumstay and Kaufman 1983). The off-source positions were chosen 10′ away from the central position of M83 and were assumed to be free of CO emission.

The receiver gain and atmospheric emission and absorption were calibrated by chopping with a room-temperature absorber (Ulich and Haas 1976). To calibrate the elevation dependence of the antenna gain, we monitored the profile at the center of M83 during integration sequences. All spectra were scaled so that the central profile in the same sequence became the same intensity as the average over all sequences.

In 1987 incompleteness of image band rejection at the single sideband (SSB) filter of the NRO 45-m telescope was found. To adjust the intensity scale of the emission we observed a few positions on and around the center of M83 again in June 1987 using a new SSB filter which completely rejects the image-band emission. Comparing the intensities of new and old observations we acquired a scaling factor of 1.55 for our observations. We use the new antenna temperature scale in this paper. The beam efficiency was 0.45 for this temperature scale.

A linear baseline fit was applied to each profile. Pointing was monitored on SiO maser star W Hya every 1 or 2 hours. The position of W Hya was $\alpha = 13^h46^m12^s.1$, $\delta = -28°7'8''$ (epoch 1950.0), only 3° from M83. The pointing accuracy was about 5″.

We mapped a 210″ × 60″ (3.8 kpc × 1.1 kpc at 3.7 Mpc) area covering the optical bar, observing 73 positions spaced by 15″ or 270 pc. In addition we observed 12 positions spaced by 7″.5 or 135 pc in the central 30″ × 15″ region. The observed positions are indicated by dots in figure 1.

3. Results

i) Spatial Distribution of the CO Emission

Figure 1 shows the distribution of integrated CO intensity and figure 2 shows the same map superposed on the optical image from the Hubble atlas of galaxies (Sandage 1961).

The most prominent CO feature is a bar-like structure along the optical bar. [The

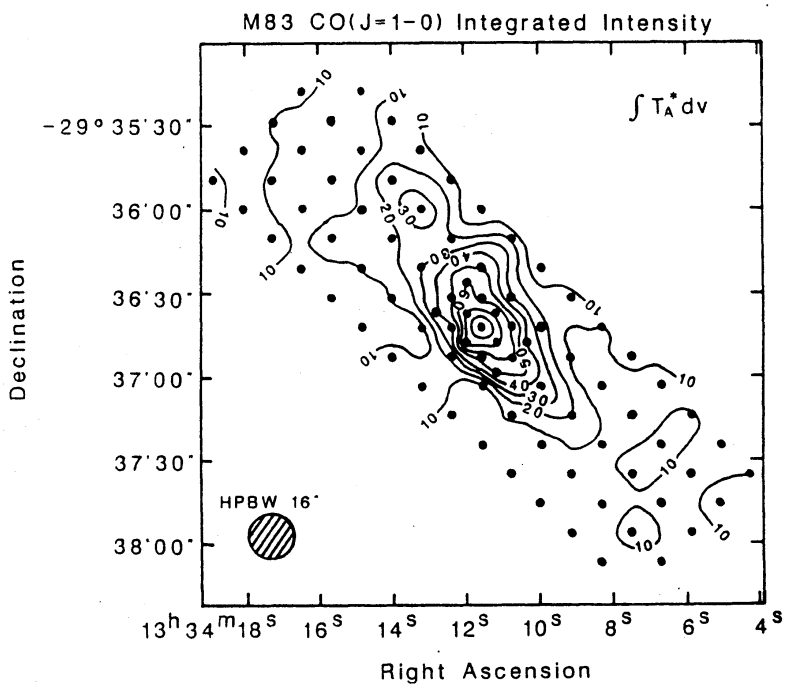

Fig. 1. The distribution of the integrated intensity between 250 − 750 km s^{-1} V_{LSR}. The contour levels are from 10 K km s^{-1} to 80 K km s^{-1} with increments of 10 K km s^{-1}. The observed positions are indicated with dots.

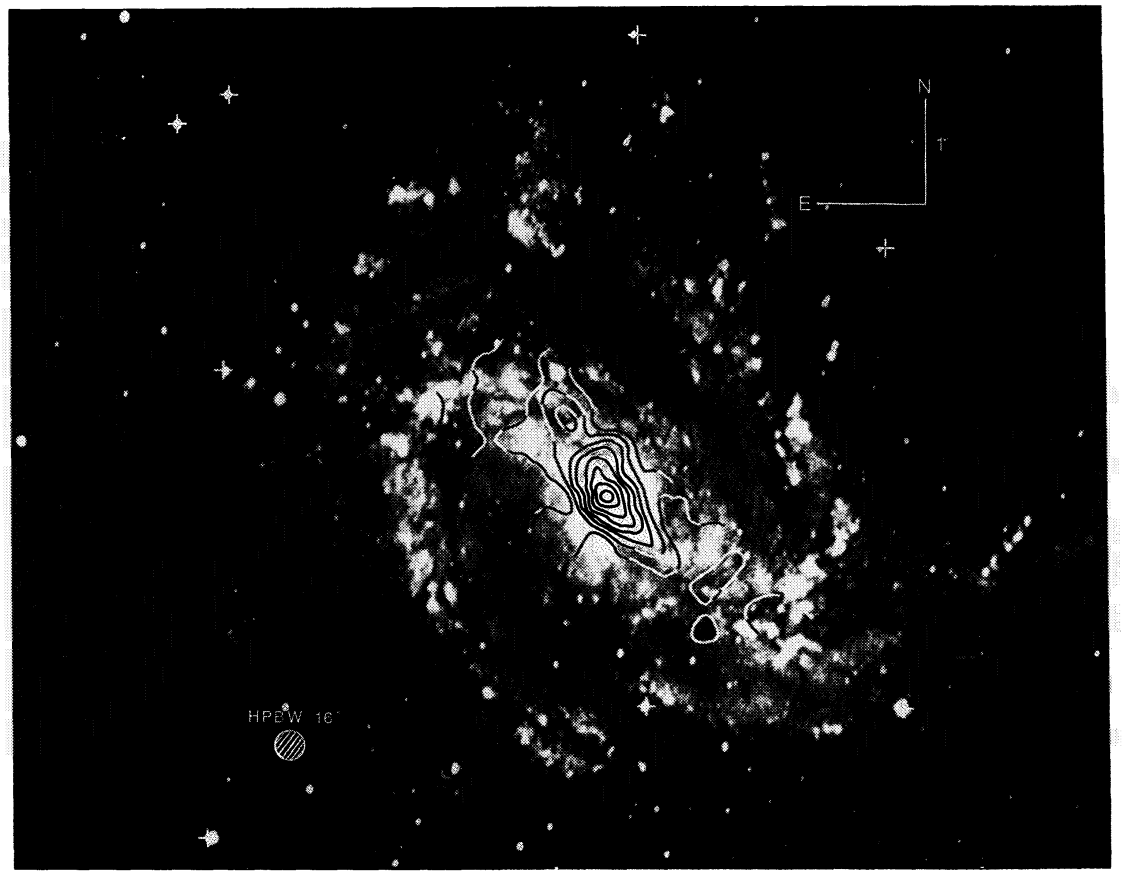

Fig. 2. The same CO map as figure 1 superposed on the optical image from the Hubble Atlas of Galaxies (Sandage 1961).

position angle of the optical bar is estimated as 43° by de Vaucouleurs et al. (1983).] We refer to it as the molecular bar in this paper. The molecular bar is not straight, but bent. The bend is more evident in the distribution of the peak antenna temperature. It is mainly due to a rather narrow linewidth at a few positions around the nucleus. Figure 3 shows a map of the peak antenna temperature. The ridge of the molecular bar is shifted from the major axis of the optical bar toward the leading side.

The CO emission is concentrated toward the center of the galaxy. The CO line fluxes in the whole observed area and in the central $45'' \times 45''$ (0.8 kpc $\times$ 0.8 kpc) region are 2.0×10^5 K km s^{-1} arcsec^2 and 8.2×10^4 K km s^{-1} arcsec^2, respectively, where we define the CO line flux as $L_{\rm CO} = \int T_{\rm A}^{*} dv\, dx\, dy$. About 40% of the CO line flux in the whole observed area is concentrated in the central $45'' \times 45''$ region. The image of the nuclear region in CO shows a high concentration of molecular gas. This high-density nuclear component is associated with two protrusions which extend in opposite directions from the nucleus toward the molecular bar. It is similar to the images in radio continuum, optical continuum, Hα line, and X-ray emission [radio continuum: Cowan and Branch (1985); Ondrechen (1985), optical continuum: Pastoriza (1975), Hα line: de Vaucouleurs et al. (1983), X-ray: Trinchieri et al. (1985)].

There are two other cloud-like concentrations at the northeastern and southwest-

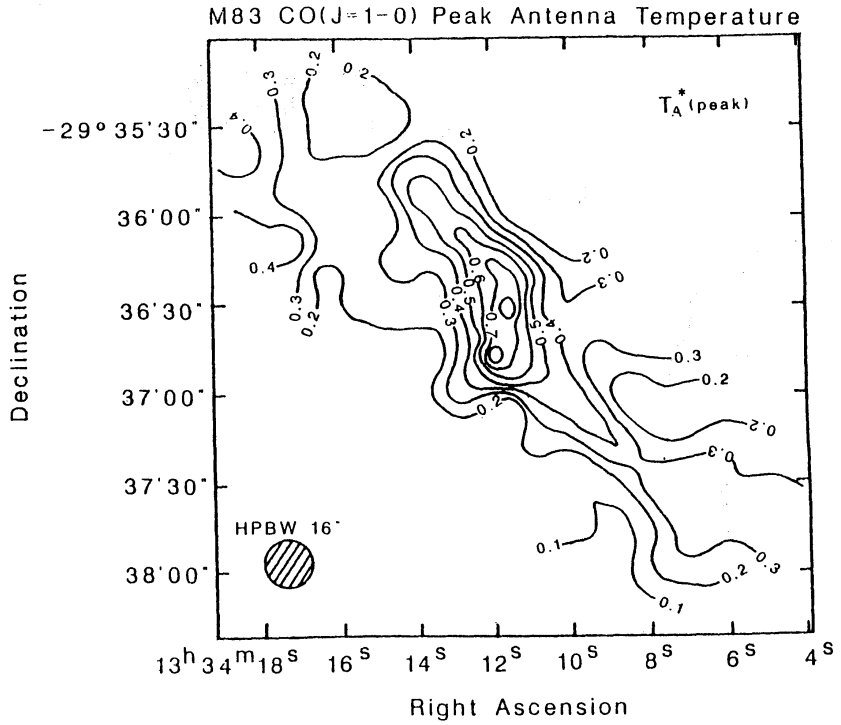

Fig. 3. The contour map of the peak CO antenna temperature. The contour levels are from 0.1 K to 0.8 K with increments of 0.1 K.

ern ends of the bar. These correspond to cusps, where the bar joins the spiral arms. The molecular clouds at the cusps may extend to the molecular cloud complex associated the dust lanes on the spiral arms.

ii) Kinematics of Molecular Gas

In order to investigate the velocity field we plotted the mean velocities in figure 4. The map was made only from those positions where the peak antenna temperatures exceeded 0.2 K.

In the nuclear region the velocity field shows a weak deviation from circular rotation. The iso-velocity contours are slightly inclined with respect to the minor axis of the galaxy. This indicates that the gas has noncircular motions, as predicted from theoretical models (e.g. figure 12 of Roberts et al. 1979). The velocity deviation across the molecular bar corresponds to about 20–40 km s^{-1} in the plane of the galaxy. In the northeastern half of the bar the velocity field shows weak evidence for noncircular motions, consistent with an inflow toward the nucleus.

The noncircular motion of gas in the nuclear region was also observed in the Hα line by Comte (1981) and Allen et al. (1983). However, the Hα observations by de Vaucouleurs et al. (1983) show no deviation from circular rotation in the nuclear region. Our results are consistent with the results of Comte (1981) and Allen et al. (1983) rather than de Vaucouleurs et al. (1983).

Figure 5 shows a position-velocity diagram along the major axis and along the minor axis. The primary feature in the major axis diagram shows that the rotation velocity rises steeply in the nuclear region ($|x| \leq 15''$) and gradually in the outer region

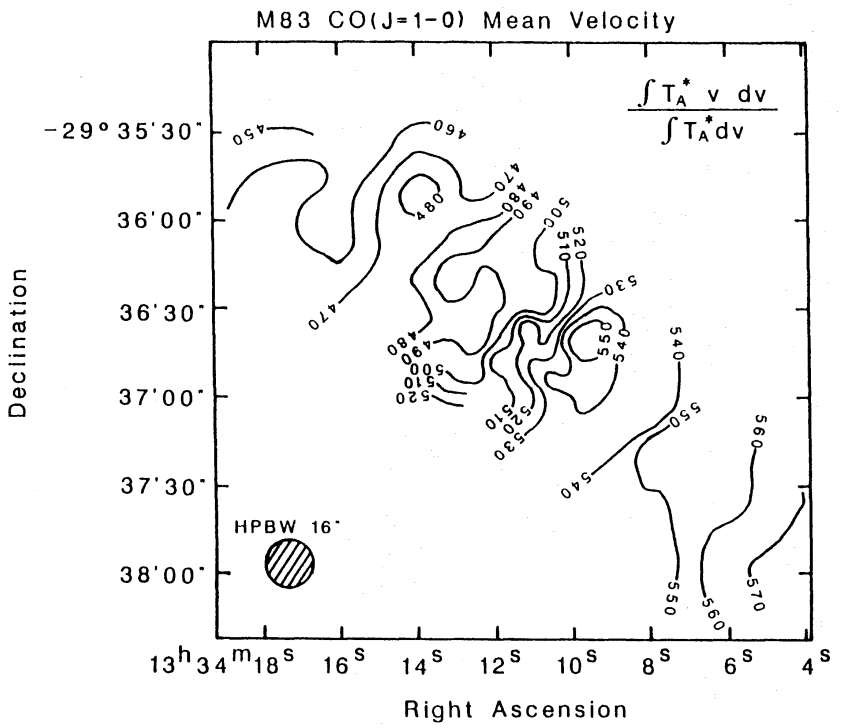

Fig. 4. The velocity field of the CO emission (mean velocity in V_{LSR}). The map was plotted from only those positions where the peak antenna temperature exceeded 0.2 K. The contour levels are from 450 km s^{-1} to 570 km s^{-1} with increments of 10 km s^{-1} step.

($|x| \geq 45''$). In the outer region, the velocity of gas increases linearly with the radius. It is well fitted by an extrapolation of the HI rotation curve (Rogstad et al. 1974, model B). The Hα velocities also agree well with the CO velocities. The steep velocity gradient in the nuclear region is hardly seen in the Hα emission. This is because the Hα velocities are mean velocities and are sampled at only a few positions within the nuclear region. The mean velocities are less sensitive to a steep velocity gradient because of the highly concentrated distribution of Hα emission. The CO emission is distributed symmetrically with respect to the assumed center ($\alpha = 13^h34^m11^s.55$, $\delta = -29°36''42''.2$) and to the $V_{LSR} = 510$ km s^{-1}. It allows us to assume that the systemic velocity is 510 km s^{-1}(V_{LSR}) and that the dynamical center coincides with the assumed center. The position-velocity diagram along the minor axis shows that the velocity gradient along the minor axis is only about 10–20 km s^{-1} over 1'.

The linewidths are significantly different in the central region and the molecular bar. In the central region ($|x| \leq 30''$) the full width at the half maximum (FWHM) of the line is about 100 km s^{-1}. At the map center ($x = 0'', y = 0''$) the emission extends from 350 km s^{-1} to 710 km s^{-1} and the full width between zeros is about 360 km s^{-1}. Figure 6 shows CO profiles at 15 positions around the map center. In the molecular bar the emission line was not as broad, with an FWHM of about 20 km s^{-1}.

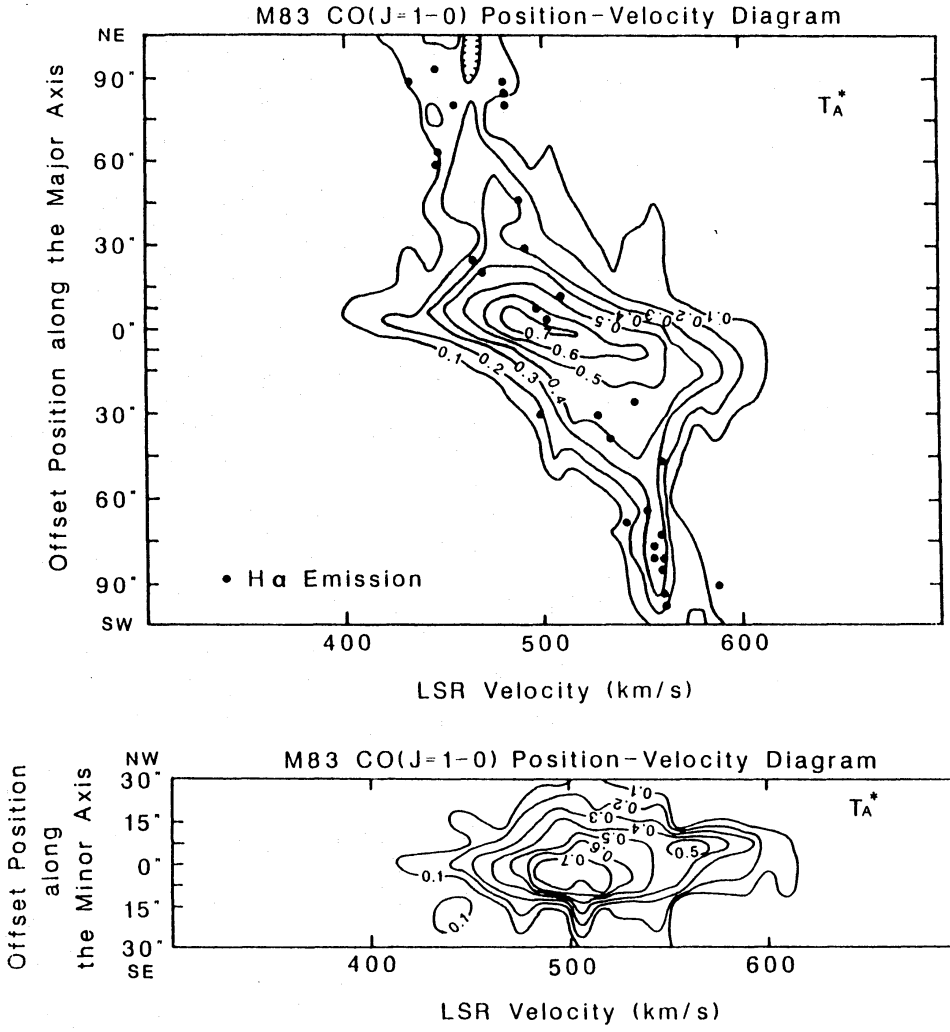

Fig. 5. (a) The position-velocity diagram along the major axis of M83 (position angle of the galaxy is 45°). The contour levels are from 0.1 K to 0.7 K with increments of 0.1 K. Northeast is at the top and southwest is at the bottom. Tick marks along the vertical axis show the observed positions. Dots show Hα velocities along the major axis. The plotted data were taken from those pixels which are crossed or touched by the line of nodes (position angle=45°) in the figure 4 of Comte (1981). (b) The position-velocity diagram along the minor axis of M83 (position angle is −45°). Northwest is at the top and southeast is at the bottom. Contour levels and tick marks are the same as the panel (a).

4. Discussion

i) The Shocked Region in the Bar

The molecular bar is the first direct evidence that molecular clouds are associated with the straight dust lane on the optical bar of barred spiral galaxies (figure 2). It is located on the leading edge of the bar potential. Figure 7 shows a CO map superposed on the K-band (2.2-μm) map (Adamson et al. 1987). Here, we shifted the position

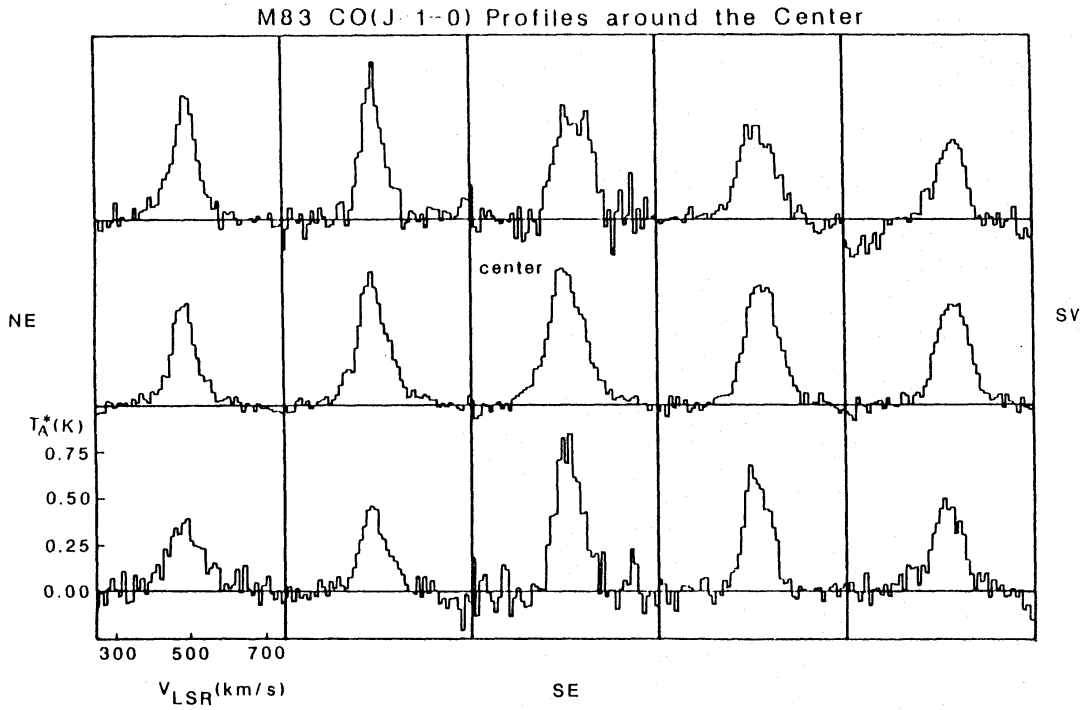

Fig. 6. The CO profiles at 15 positions around the map center. Left is northeast and top is northwest. Sample spacing is 7″.5. Note the broad linewidth and extended velocity wing.

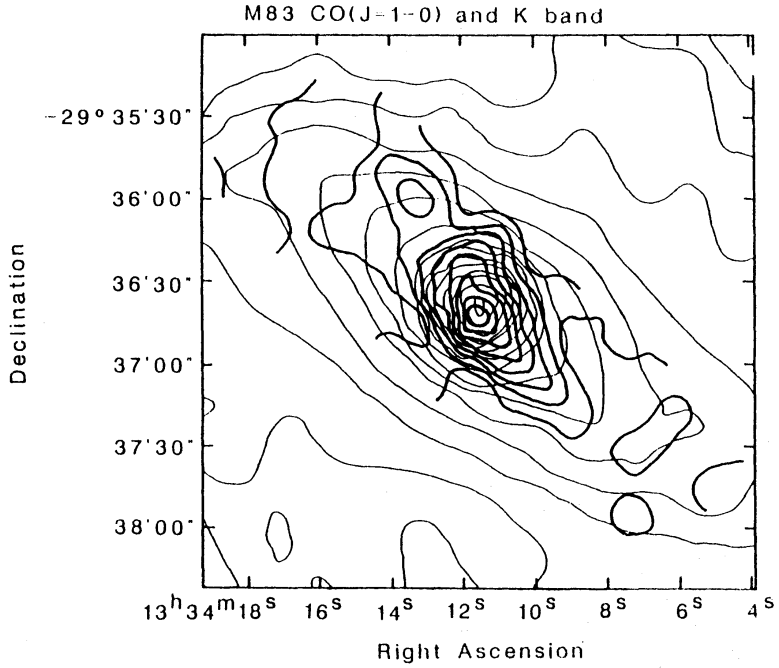

Fig. 7. A superposition of the contour map of the integrated intensity of the CO emission (thick contours, the same as figure 1) on the K-band image (thin contours) of Adamson et al. (1987) (the K-band image was shifted as mentioned in the text). The molecular bar exists just at the leading edge of the bar potential, which is traced by the light in the K-band image.

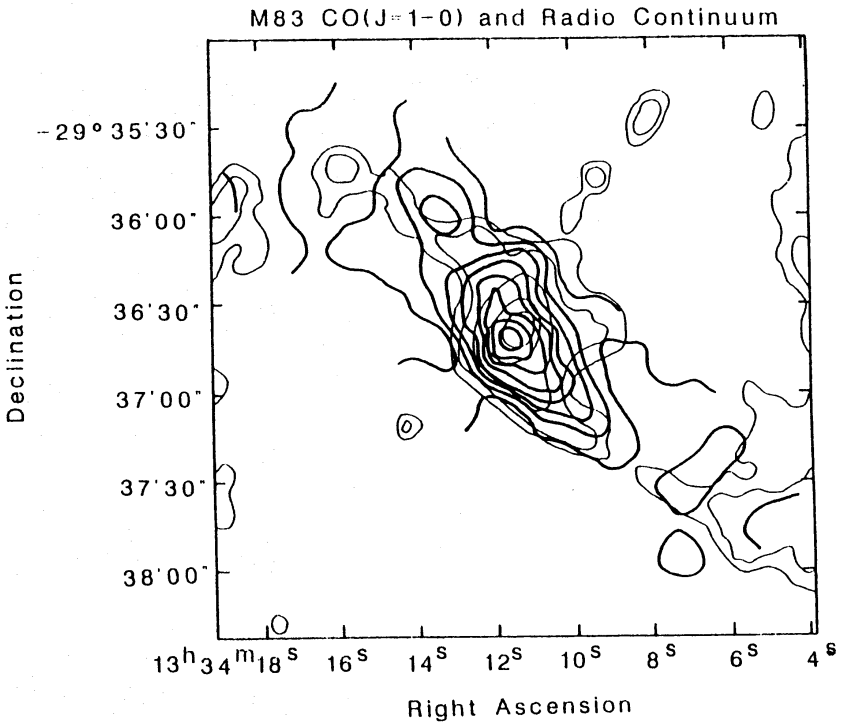

Fig. 8. A superposition of the contour map of the integrated intensity of the CO emission (thick contours, the same as figure 1) on the radio continuum emission at 4885 MHz (thin contours) of Ondrechen (1985). The good correlation of the distributions suggests gas compression in the bar and a very active star forming complex in the nucleus.

of the K-band image by $1^s.5$ toward the east and $8''$ toward the north, using the positions of a star at $\alpha = 13^h34^m9^s.7$ $\delta = -29°38'37''$ in an optical image and of the corresponding point source in the J-band image of Adamson et al. (1987). The figure shows that the molecular bar is located in the leading edge of the bar in the K-band image. This shows that molecular clouds are concentrated on the leading edge of the bar potential, because the K-band image shows old population stars which trace the stellar mass distribution. This is consistent with the theoretical prediction.

The distributions of the CO and radio continuum emission (Ondrechen 1985) are well correlated (figure 8), where the continuum emission is mostly nonthermal. This is consistent with gas compression in the bar because the nonthermal radio continuum emission is enhanced when magnetic fields are compressed. The comparison shows that molecular gas is accumulated at the leading edge of the bar as suggested by theoretical models.

The bar is less prominent in Hα emission, even though molecular gas is concentrated there (figure 9). This means that interstellar gas is accumulated in the bar by a shock, whereas stars are not formed there efficiently, indicating that the star-forming efficiency in the bar is lower than in the nucleus. This suggests that the accumulated molecular gas is not consumed in the bar but, rather, flows into the nucleus.

The kinematics of the CO gas is also consistent with the theoretical models of a barred galaxy. The noncircular motion in the nuclear region suggests elliptical orbits and inflow toward the nucleus. The concentration of the CO emission toward the

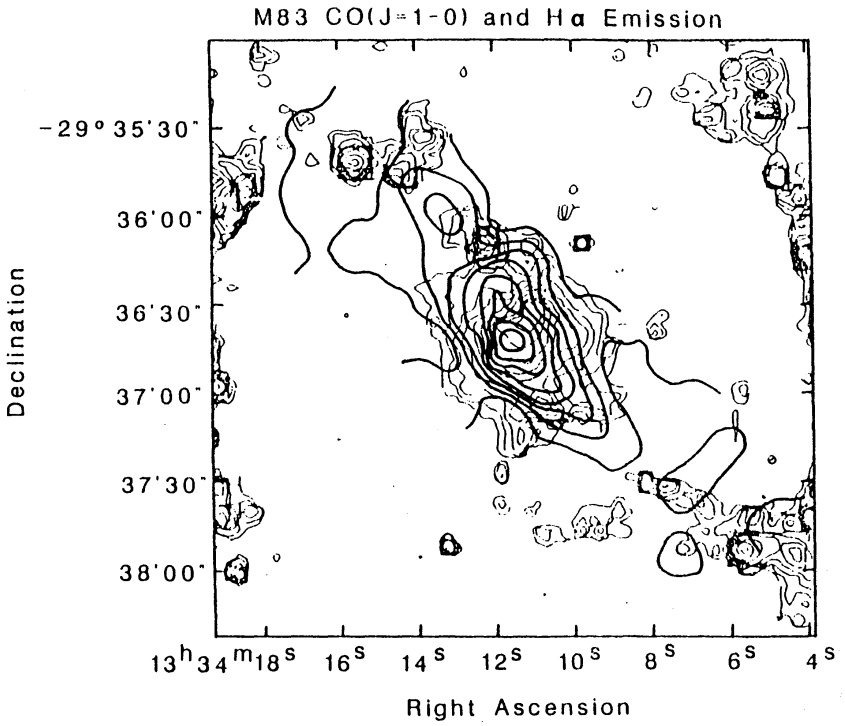

Fig. 9. A superposition of the contour map of the integrated intensity of the CO emission (thick contours, the same as figure 1) on the Hα emission (thin contours) of de Vaucouleurs et al. (1983). The bar is less prominent in the Hα emission although molecular gas is concentrated. The peak in the Hα emission is shifted from the peak in the CO emission by about 10″ toward the northwest.

nucleus supports the gas inflow model.

The morphological similarity of the nuclear region in CO, Hα, and radio continuum suggests that the nuclear region is a giant complex of star-forming sites. This suggests that the nuclear activity in M83 is due to an active star formation over an extended area. This may be due to the gas inflow which is suggested by the observations and predicted by theoretical models. The inward flow of the molecular gas should supply raw material for continuous active star formation in the nucleus. The two protrusions of the nucleus toward the molecular bar may be channels of gas inflow.

The CO peak does not coincide with the Hα peak. The difference is about 10″, which is larger than the pointing error of our observations. The disagreement may be due to an inhomogeneity of the star-forming activity within the nuclear region and/or heavy absorption of the Hα light by dust in molecular clouds.

ii) Mass of the Molecular Gas

To estimate the mass of the molecular gas of M83, we use the empirical relation between integrated ^{12}CO intensity and H_2 column density, that is

$$N(\mathrm{H_2}) \cong 4 \times 10^{20} \int T_\mathrm{R} dv [\mathrm{H_2 cm^{-2}}], \quad (1)$$

where T_R is the radiation temperature in Kelvin, and v is the line velocity in km s^{-1} (Young and Scoville 1982) [Kutner and Ulich (1981) showed that T_A^* taken by

the Cassegrain focus receiver on the NRAO 11-m telescope is almost the same as $T_R{}^*$, and for galactic clouds T_R is nearly equal to $T_R{}^*$ because galactic clouds are extended beyond the main beam of the telescope]. For M83 T_R should be close to mean brightness temperature in the telescope main beam ($T_{mb} = T_A{}^*/\eta_{mb}$), rather than $T_R{}^*$, since the distribution of CO emission of M83 is highly concentrated toward the center (section 3-i). In this paper we use the relation (1) and assume T_R is equal to the mean brightness temperature in the main beam to estimate the H_2 masses.

The H_2 masses in the whole observed area and in the central 15″(270-pc)-radius region derived from the integrated ^{12}CO intensity are 9×10^8 $M_\odot$ and 2×10^8 $M_\odot$, respectively. The mass of gas estimated from the dust mass in the nucleus with a 30″-beam is 4×10^7 $M_\odot$ [Telesco and Harper (1980): adjusting the distance to 3.7 Mpc and assuming the interstellar gas-to-dust ratio, $M(\text{gas})/M(\text{dust}) = 4.5 \times 10^2$ from Young et al. (1986) instead of 10^2 because infrared flux measured by Telesco and Harper (1980) dominated by emission from warm dust]. The discrepancy of a factor of 5 between the molecular masses in the 15″-radius region derived from ^{12}CO intensity and from dust mass may arise because of the following three large ambiguities. One is the uncertainty of the relation (1) itself, which is by about a factor of two (Young and Scoville 1982). Another is due to the gas temperature difference between molecular clouds in a disk and in a nucleus. At the nucleus of a galaxy the gas temperature should be significantly higher than in the galactic disk. The CO luminosity is proportional to the averaged temperature of molecular clouds in a beam (Young et al. 1986). The conversion factor of relation (1) should be smaller when the gas temperature is significantly higher than that of the molecular clouds in the disk. If this is the case, the mass of molecular gas derived using relation (1) will be overestimated. The third is the uncertainty of the total dust mass. Telesco and Harper (1980) assumed that the dust temperature of M83 was the same as that of M82, which is 45 K, and estimated the dust mass for the single temperature component. If the averaged dust temperature of M83 is lower than that of M82, then the estimated dust mass will increase. If the dust temperature of M83 is assumed to be the same as that of NGC 253, which is 40 K (Telesco and Harper 1980), the derived dust mass will increase by a factor of 1.8.

The lower limit of H_2 mass can be estimated by assuming that the ^{12}CO line is optically thin. The H_2 mass (the lower limit) in the central 15″-radius region is $3 \times 10^6 M_\odot$, if $N(^{13}\text{CO})/N(^{12}\text{CO}) = 1/89$ (Turner 1974) and $N(H_2)/N(^{13}\text{CO}) = 5 \times 10^5$ (Dickman 1978), and the excitation temperature of CO is 40–45 K.

The stellar mass in the central 15″-radius region is $1.3 \times 10^9 M_\odot$ (Jensen et al. 1981). The mass fraction of molecular gas in the central 15″-radius region is, therefore, 0.2% for the model for an optically thin CO line and 14% for an empirical relation (1).

iii) The Steep Velocity Gradient and the Large Velocity Dispersion around the Nucleus

The position-velocity diagram (figure 5) shows a steep velocity gradient along the major axis in the nuclear region ($|x| \leq 7.''5$) but a gentle gradient along the minor axis. The symmetric feature around the nucleus in the position-velocity diagram suggests that this steep gradient is due to a fast rotating component. To confirm this and to derive the rotation curve without resolution effects, we made a kinematical model of the galaxy. We assumed that the molecular gas distribution is axisymmetric and

the rotation is circular. The mass derived from this rotation curve is correct only to an order of magnitude, because there is the observed velocity deviation from circular rotation of about 20 km s^{-1} and the rotation velocity is larger than 80 km s^{-1} except for the 5″-radius region (see chapter 3 and the best fit rotation curve derived later). Discussion about precise mass distribution is beyond the scope of this paper. The distribution of the integrated CO emission can be fit by a combination of a Gaussian core and an exponential disk (the peak ratio of the gaussian core and the exponential disk was taken to be 136: 19 from our data, the FWHM of the core was taken to be 18″ from our data, and the e-folding length of the disk was taken to be 120″ from the near infrared data of Adamson et al. 1987). The intrinsic velocity dispersion was assumed to be a three-dimensional isotropic Gaussian distribution. The rotation curve and the FWHM of the velocity dispersion were searched in order to find the best fit to M83. To simplify the kinematical model, we restricted the rotation curve to be the simplest one, having only three parameters. The derived rotation curve assumes a sphere with a constant density core surrounding a constant density halo under virial equilibrium, which can be characterized by the core radius, the core density, and the halo density. The FWHM of the velocity dispersion was assumed to decrease exponentially, because we could not reproduce the CO distribution in the position-velocity diagram by any model with a constant velocity dispersion.

We have calculated the position-velocity diagram along the major axis of the kinematical model, considering the finite beam size (HPBW=16″) and the inclination of the disk ($i = 24°$) but neglect the projected distance on the sky from the galactic plane. Figure 10 shows the position-velocity diagram which is the most similar to the

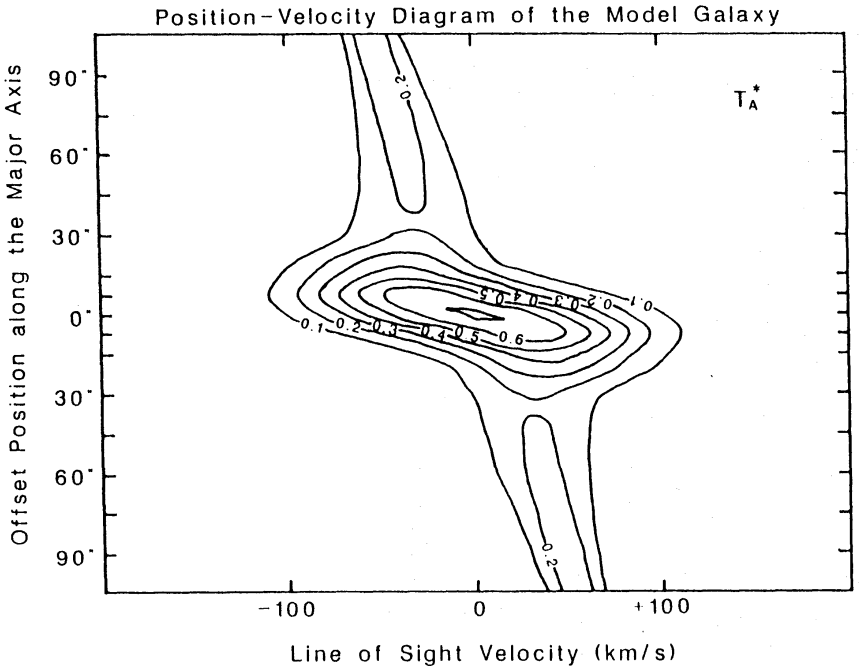

Fig. 10. The position-velocity diagram of the kinematical model along its major axis. The inclination of the model was set to 24°, which is the same as that of M83. The parameters of the model galaxy are summarized in table 2 and shown in figure 11. Tick marks along the vertical axis show positions where profiles were synthesized.

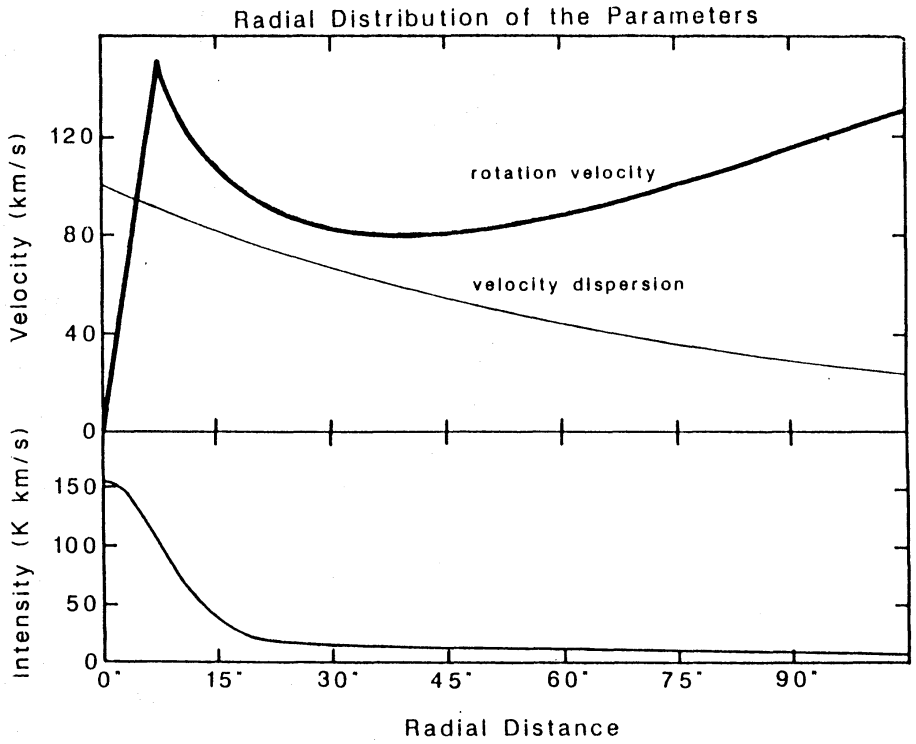

Fig. 11 Radial distributions of the parameters of the kinematical model. Thick line in the upper panel shows the rotation curve, which is the same shape as the virial equilibrium velocity of spherical distribution of mass with a uniform density core surrounding a uniform density halo. The thin line in the upper panel shows the FWHM of the velocity dispersion, which is assumed to be a three-dimensional isotropic gaussian distribution. The lower panel shows the distribution of the CO integrated intensity from the fit of the integrated intensity map (figure 1).

observed one of M83 (figure 5). The parameters of the best fit model are summarized in table 2 and shown in figure 11. The synthesized profiles along the minor axis of the kinematical model were also similar to the observed profiles of M83.

From the model calculations we conclude that the rotation curve of M83 rises very steeply in the nucleus ($r \leq 7''.5$ or 130 pc) and falls steeply out of the nucleus. This directly indicates that there is a very high contrast of densities between the nucleus and the outer region, which our model suggests is a factor of $\sim$ 300. The best-fit rotation curve suggests that the radius of the dense region is 130 pc. This core mass is approximately $10^9 M_\odot$.

The high-velocity dispersion of molecular clouds in the nuclear region may be due to active star formation. The kinetic energy required to explain the observed velocity dispersion in the $r \leq 15''$ region is 10^{54}–10^{55} ergs. It could possibly be supplied by supernova explosions. Bohlin et al. (1983) estimate the supernova rate of the core of M83 by scaling a model of Rieke et al. (1980) using far infrared luminosity of the central 40″-diameter region of M83 measured by Telesco and Harper (1980) (adjusting the distance of M83 to 3.7 Mpc). The inferred supernova rate of the core of M83 is $0.01 - 0.02\mathrm{yr}^{-1}$. A typical supernova explosion gives 10^{49} ergs of kinetic energy to dense interstellar matter (Chevalier 1974). X-ray observations suggest the burst of star formation began about 10^7 yr ago (Trinchieri et al. 1985). If a constant supernova

Table 2. Parameters of the kinematical model.

(i) Fixed parameters	
Gas distribution	Axisymmetric infinite-thin disk
Gas motion	Circular rotation
Inclination of the disk ...	24°
Surface density of the integrated intensity	
Gaussian core	Peak..... 136 K km s^{-1}
	FWHM ..... 18″
Exponential disk	Peak ..... 19 K km s^{-1}
	Scale length ... 120″
Shape of the rotation curve	
Virial equilibrium velocity of spherical distribution of mass with a uniform core and a uniform halo	
Random velocity dispersion	
Three-dimensional isotropic gaussian distribution of which FWHM decreases exponentially with the radius	
(ii) Fitted parameters	
Rotation curve	
Core radius.....	7.5″ = 1.3 $\times 10^2$ pc
Peak rotation velocity ...	150 kms^{-1}
Density ratio.....	0.0035
Velocity dispersion	
FWHM at the center.....	100 km s^{-1}
Scale length of decrease...	75″ =1.3 $\times$ 10^3 pc

rate is assumed over the last 10^7 yr, 10^{54} erg of kinetic energy can be provided to dense interstellar matter by supernova explosions. This is consistent with the kinetic energy of velocity dispersion in the nucleus. The smaller velocity dispersion in the outer region may be due to a lower frequency of supernovae.

5. Conclusion

In this paper we have presented the distribution of the CO line emission in the central region and the bar of the intermediate barred spiral galaxy M83 with a 16″-beam. The conclusions are summarized as follows.

(1) The molecular gas is concentrated in a "molecular bar", which is along the optical bar. The ridge of the molecular bar is bent and located on the leading edge of the bar potential. This is the first direct evidence that the molecular clouds are concentrated on the leading edge of the bar of a barred spiral galaxy.

(2) A large concentration of molecular gas is observed in the nucleus. About 40 percent of the CO line flux from the whole observed area of 210″ × 60″ (3.8 kpc × 1.1 kpc) is concentrated in the central 45″ × 45″ (0.8 kpc × 0.8 kpc) region.

(3) The velocity field of the CO gas shows noncircular rotation, suggesting oval motions and inflow of gas into the nucleus.

(4) The distribution and kinematics of the molecular gas are consistent with the prediction of the theoretical models of barred spiral galaxies.

(5) The CO position-velocity diagram along the major axis shows a sharp increase in velocities near the nucleus of the galaxy. Large linewidths with asymmetric profiles are observed near the nucleus along the major axis. These observations are explained if the rotation curve rises steeply in the nucleus and the velocity dispersion is $50-100$ km s^{-1} around the nucleus.

We thank S. Ichikawa and T. Aoki of the Kiso Observatory of the University of Tokyo for their help in measuring the positions of reference stars for figure 2. We thank the referee for useful suggestions and advices. T.H. and N.N. are indebted to the Japan Society for the Promotion of Science for the financial support.

References

Adamson, A. J., Adams, D. J., and Warwick, R. S. 1987, *Monthly Notices Roy. Astron. Soc.*, **224**, 367.

Allen, R. J., Atherton, P. D., Oosterloo, T. A., and Taylor, K. 1983, in *IAU Symp. 100, Internal Kinematics and Dynamics of Galaxies*, ed. E. Athanassoula (D. Reidel Publishing Company, Dordrecht), p. 147.

Bohlin, R. C., Cornett, R. H., Hill, J. K., Smith, A. M., and Stecher, T. P. 1983, *Astrophys. J. Letters*, **274**, L53.

Chevalier, R. A. 1974, *Astrophys, J.*, **188**, 501.

Combes, F., Encrenaz, P. J., Lucas, R., and Weliachew, L. 1978, *Astron. Astrophys.*, **67**, L13.

Comte, G. 1981, *Astron. Astrophys. Suppl.*, **44**, 441.

Cowan, J. J., and Branch, D. 1985, *Astrophys. J.*, **293**, 400.

de Vaucouleurs, G. 1979, *Astron. J.*, **84**, 1270.

de Vaucouleurs, G., de Vaucouleurs, A., and Corwin, H. 1976, *Second Reference Catalogue of Bright Galaxies* (University of Texas Press, Austin).

de Vaucoulers, G., Pence, W. D., and Davoust, E. 1983, *Astrophys. J. Suppl.*, **53**, 17.

Dickman, R. L. 1978, *Astrophys. J. Suppl.*, **37**, 407.

Huntley, J. M., Sanders, R. H., and Roberts, W. W., Jr. 1978, *Astrophys. J.*, **221**, 521.

Jensen, E. B., Talbot, R. J., Jr., and Dufour, R. J. 1981, *Astrophys. J.*, **243**, 716.

Kutner, M. L., and Ulich, B. L. 1981, *Astrophys. J.*, **250**, 341.

Lord, S. D., Strom, S. E., and Young, J. S. 1987, in *Star Formation in Galaxies*, ed. C. J. L. Persson (NASA CP2466) p. 303.

Ondrechen, M. P. 1985, *Astron. J.*, **90**, 1474.

Pastoriza, M. G. 1975, *Astrophys. Space Science*, **33**, 173.

Prendergast, K. H. 1983, in *IAU Symp. 100, Internal Kinematics and Dynamics of Galaxies*, ed. E. Athanassoula (D. Reidel Publishing Company, Dordrecht), p. 215.

Rickard, L. J., Palmer, P., Morris, M., Turner, B. E., and Zuckerman, B. 1977, *Astrophys. J.*, **213**, 673.

Rieke, G. H. 1976, *Astrophys. J. Letters*, **206**, L15.

Rieke, G. H., Lebofsky, M. J., Thompson, R. I., Low, F. J., and Tokunaga, A. T. 1980, *Astrophys. J.*, **238**, 24.

Roberts, W. W., Jr., Huntley, J. M., and van Albada, G. D. 1979, *Astrophys. J.*, **233**, 67.

Rogstad, D. H., Lockhart, I. A., and Wright, M. C. H. 1974, *Astrophys. J.*, **193**, 309.

Rumstay, K. S., and Kaufman, M. 1983, *Astrophys. J.*, **274**, 611.

Sandage, A. 1961, *The Hubble Atlas of Galaxies*, (Carnegie Institution of Washington, Washington).
Sérsic, J. L., and Pastoriza, M. 1965, *Publ. Astron. Soc. Pacific*, **77**, 287.
Sørensen, S.-A., Matsuda, T., and Fujimoto, M. 1976, *Astrophys. Space Science*, **43**, 491.
Talbot, R. J., Jr., Jensen, E. B., and Dufour, R. J. 1979, *Astrophys. J.*, **229**, 91.
Telesco, C. M., and Harper, D. A. 1980, *Astrophys. J.*, **235**, 392.
Trinchieri, G., Fabbiano, G., and Paulumbo, G. G. C. 1985, *Astrophys. J.*, **290**, 96.
Turner, B. E. 1974, in *Galactic and Extragalactic Radio Astronomy*, ed. G. L. Verschuur and K. I. Kellermann (Springer-Verlag, Berlin), p. 199.
Ulich, B. L., and Haas, R. W. 1976, *Astrophys. J. Suppl.*, **30**, 247.
Young, J. S., and Scoville, N. 1982, *Astrophys. J.*, **258**, 467.
Young, J. S., Schloerb, F. P., Kenney, J. D., and Lord, S. D. 1986, *Astrophys. J.*, **304**, 443.